Photocatalytically reactive surfaces for simultaneous water harvesting and treatment

Ritwick Ghosh [1,2], Adrien Baut [1], Giorgio Belleri [1], Michael Kappl [2], Hans-Jürgen Butt [2] & Thomas M. Schutzius [1,3] ✉

Atmospheric water harvesting provides decentralized and sustainable supplies of fresh water in areas away from natural water resources. However, an important challenge is that water sources such as fog are subject to contamination from airborne pollutants, especially near population centres. Here we demonstrate a rationally designed system that can capture fog at high efficiency while simultaneously degrading organic pollutants. At the heart of our design is a wire mesh coated with anatase titanium dioxide nanoparticles embedded in a polymer matrix. Once activated by sunlight, the photoactive titanium dioxide layer decomposes organic molecules such as diesel, even in the absence of sunlight; moreover, the wettability of the mesh surface is engineered to enhance water extraction. In outdoor tests, the device can maintain a good fog harvesting performance as well as a water treatment efficiency of >85%. The continuous production of water with passive purification demonstrated in our study provides an energy-free solution to address water scarcity.

Most of the global population is living under conditions where freshwater consumption exceeds replenishment during at least one month of the year[1]. Currently, there is enough fresh water available globally to meet demand; however, scarcity arises due to uneven distribution[2,3] and contamination[4,5]. To address this challenge, the focus of research over the past few decades has been on the atmospheric water harvesting of sources such as rain[6], fog[7–9], dew[10,11] and vapour[12,13] as well as reducing freshwater use[14,15] and treating contaminated water sources[16]. The emphasis has been on creating energy-neutral atmospheric water harvesting processes[17,18], such as deploying meshes to collect fog[7,8], the radiative cooling of surfaces to condense dew[10,11] and using solar-activated sorbents to adsorb and release water vapour[12,13]. Of these, fog harvesting is one of the most promising methods: a mesh of one square metre can harvest 9–70 litres per day at urban locations (for example, in Lima, Peru and in Dhofar, Oman)[8,19], and large-scale installations (that is, 5,000 m² mesh) can harvest up to 100,000 litres

of water in a single day[19]. However, the utility of this water is limited by atmospheric pollution, especially near cities where potable water is most needed[4,20].

Passive fog harvesting devices (termed fog harvesters) typically use woven fibres (for example, a Raschel mesh[19]), wire meshes[8] or wire patterns (for example, a harp[21]), and these devices are suspended and allow wind with entrained fog droplets (mean droplet diameter: 10–20 μm (ref. 22)) to pass through them. Here we refer to mesh fibres and wires summarily as 'wires' and their arrangements as 'wire patterns'. During operation the fog droplets impact and attach to the wires due to capillarity, grow due to coalescence, and drain due to gravity into a collector below. Researchers have identified several approaches to improve fog harvesting yields based on the interplay of fog droplet hydrodynamics and mesh structures or wettability. To increase the number of droplets that impact on the wires, the optimum projected surface area has been determined, which is dependent on

[1]Laboratory for Multiphase Thermofluidics and Surface Nanoengineering, Department of Mechanical and Process Engineering, ETH Zurich, Zurich, Switzerland. [2]Department of Physics at Interfaces, Max Planck Institute for Polymer Research, Mainz, Germany. [3]Department of Mechanical Engineering, University of California, Berkeley, CA, USA. ✉e-mail: tschutzius@berkeley.edu
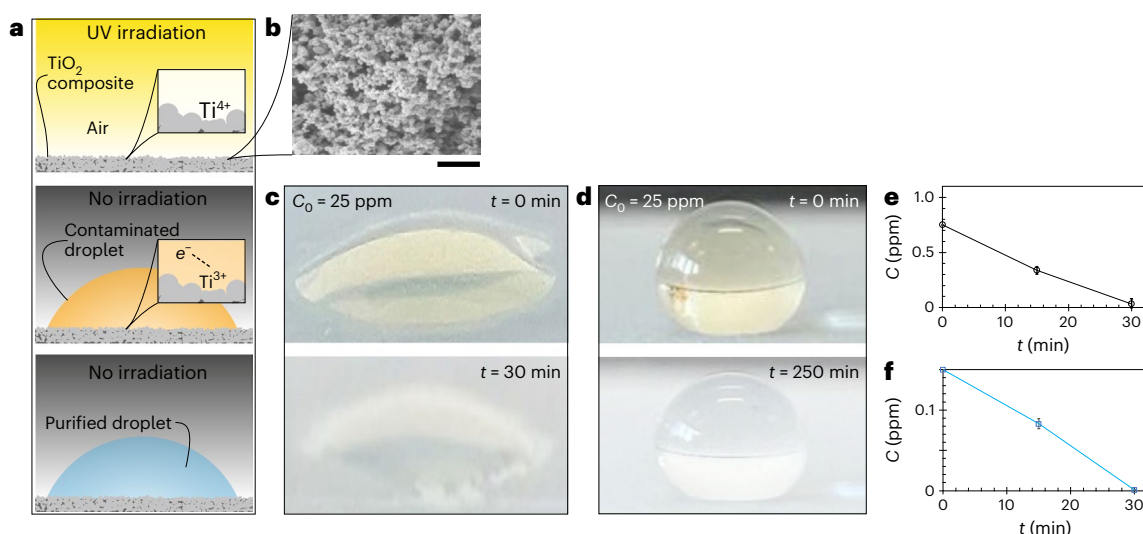
Fig. 1 | Reactive coatings that purify using intermittent UV irradiation.
a, Schematic showing how a TiO₂ nanocomposite coating can be activated by
UV irradiation and remain reactive even in the dark, enabling the purification
of water without continuous illumination from sources such as the Sun. e^-,
electron. **b**, Micrograph showing the TiO₂-nanoparticle-laden coating (TiO₂-
PVB-PDMS). Scale bar, 200 nm. **c,d**, Image sequences showing how the reactive
coatings TiO₂-PVB-PDMS (**c**) and TiO₂-EC-PDMS (**d**) can treat contaminated water
droplets (C_0 = 25 ppm methyl orange, dispensed droplet size V = 5 µl). Before
these experiments, the coatings were irradiated with UV light, photocatalytically
activating them; the coatings and droplets were not exposed to UV light thereafter.
e, Plot of concentration versus time (C–t) (black line with circle symbols)

for diesel dispersed in water. Here, the water–diesel solution was placed in a
Petri dish (diameter 42 mm; liquid volume 100 µl) that was coated with the
pre-activated TiO₂-PVB-PDMS coating. (Appropriate control experiments were
carried out to ensure that the emulsion was stable during the analysis—these
are reported in Supplementary Fig. 2.) **f**, Plot of C versus t (blue line with square
symbols) for a bisphenol A–water solution in a Petri dish coated with pre-
activated TiO₂-PVB-PDMS (liquid volume 3,000 µl). In **e** and **f**, each data point
represents the average of n = 15 measurements (that is, five readings each for
three separately prepared coating types) and the data are presented as the mean
value ± standard deviation.

the diameter of the mesh wire and the wire spacing[23]. However, the
ratio of the droplet size to the wire diameter is also equally important
in improving the collection efficiency[24]. Other important considera-
tions are the type of wire pattern[25,26] as well as the mesh material (for
example, polymer or metal), especially for mechanical robustness[27,28].
To prevent the intercepted droplets from being re-entrained into the
air flow, previous work has focused on engineering the wire surface to
have low contact angle hysteresis with a low receding contact angle[24].
The wire surfaces have also been engineered to control the transport
of droplets to the collector—avoiding over accumulation and mesh
clogging—by imparting Laplace pressure gradients[29–31], wettability
patterns[32,33] and asymmetric structures[34,35]. Through this and related
work, researchers have developed a rational approach to the design of
fog harvesters, with reported maximum collection efficiencies being
between around 12% and 17% for laboratory-scale experiments at low
wind speeds[21,24,26]. However, this work was carried out using uncon-
taminated fog, although in many applications the fog is polluted or
the water-collecting surface is fouled.

Organic pollutants are often present in fog droplets, with concen-
trations ranging from 0.3 to 25 ppm (refs. 36–38), especially near cities
where water scarcity is most acute. Previous work has used anatase
titanium dioxide (TiO₂), the most photocatalytically active phase, to
clean surface contaminants[39–41] and microbial organic deposits[42–44].
When TiO₂ is irradiated with ultraviolet (UV) light[45], this causes it to
form valence band holes that drive the catalytic decay reaction. The
limited research[46] that has been carried out using fog harvesters to
collect and treat organic-contaminated fog found that it is possible
to achieve both using mesh coatings that contain photocatalytically
active metal oxide nanoparticles such as TiO₂. However, the TiO₂-
coated mesh required active and continuous irradiation using a
UV lamp to purify water (with <36% organic content removed) and
the fundamentals of the device operation were not explored[46].

Here we show a combined fog harvesting and water purification
device that operates completely passively outdoors, requiring sunlight
only for activation. The device is constructed by embedding photocata-
lytically active TiO₂ nanoparticles in a polymer coating on the surface of
a wire mesh. The coating remains reactive even when not irradiated for
several hours, enabling the simultaneous collection and treatment of
polluted fog, even when solar irradiance is low, as it would be under foggy
conditions. Guided by wetting and diffusion–adsorption–reaction
theories, and using epifluorescence and ultraviolet-visible (UV-vis)
spectroscopy, we investigate the effect of the contaminant type and
concentration on the decay of organic compounds in water droplets
and films, and identify the rate-limiting steps, providing the necessary
basis for rational surface design. Using a rationally engineered wire
mesh coating that was pre-activated with UV light, we demonstrate
a good fog harvesting performance (~8%) and exceptional organic
pollutant reduction values of 85% and 94% when the UV index is low
and high, respectively, during outdoor tests. This coating also passively
treats water contaminants such as diesel or bisphenol A, underpinning
the possibility of using such a concept in a real-world environment
against a range of pollutants.

Results
Engineering photocatalytically reactive coatings
We engineered photocatalytic reactive coatings, one hydrophilic and
one hydrophobic, which are expected to have different water treatment
and fog harvesting performance characteristics, and we deposited
these coatings onto glass substrates and wire meshes (see Supplemen-
tary Fig. 1a,b for micrographs of the coatings). The hydrophilic photo-
catalytic reactive coating consisted of TiO₂ nanoparticles embedded in
a polyvinyl butyral (PVB) matrix with a grafted polydimethylsiloxane
(PDMS) brush. We made the coating reactive by exposing it to a UV light
source before testing (Fig. 1a,b; see also Methods). The same process
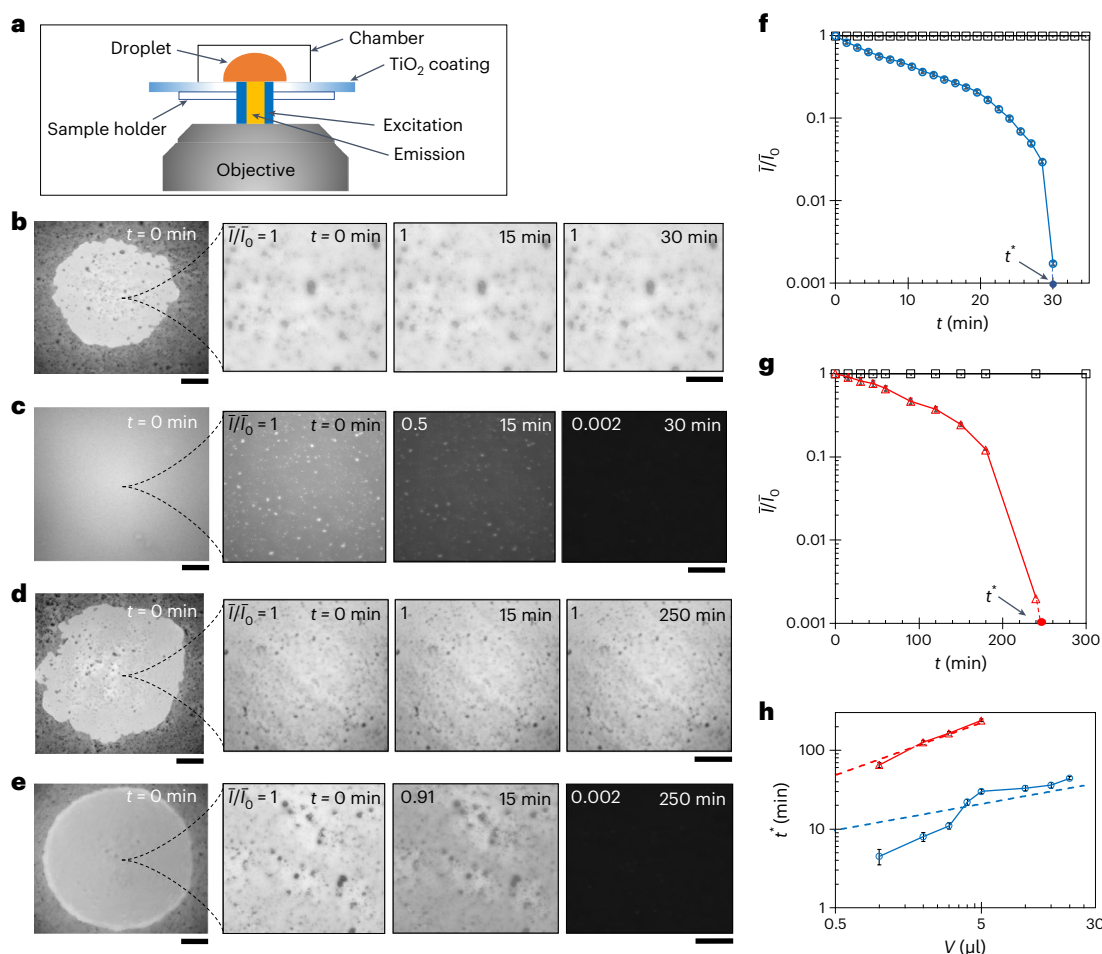
Fig. 2 | Epifluorescence microscopy to visualize the decomposition of organic contaminants on reactive coatings. a, Schematic of the microscope setup. **b**–**e**, Epifluorescence image sequences of contaminated water drops ($V = 5\,\mu l$) containing fluorescein (initial concentration, $C_0 = 25$ ppm) on the different coatings on glass substrates: TiO$_2$-PVB-PDMS surface before (**b**) and after (**c**) UV irradiation; TiO$_2$-EC-PDMS surface before (**d**) and after (**e**) UV irradiation. The TiO$_2$-PVB-PDMS and TiO$_2$-EC-PDMS coatings are hydrophilic and hydrophobic, respectively, after UV activation (Table 1). In the upper left of each image in the time sequence is shown the measured $\bar{I}/\bar{I}_0$ value, that is, the mean intensity value ($\bar{I}$) measured in the central area of the droplet–substrate interface normalized by the initial value ($\bar{I}_0$). Scale bars: primary image, 200 μm; inset sequence images, 25 μm. **f**, Plot of $\bar{I}/\bar{I}_0$ versus time (t) for the experiments in **b** (black square symbols)

and **c** (blue circle symbols). We define the decay time (t^*) as the moment when $\bar{I}/\bar{I}_0 = 0.001$, which we assume corresponds to ~99.9% reduction of the fluorescein concentration. **g**, Plot of $\bar{I}/\bar{I}_0$ versus t for the experiments in **d** (black square symbols) and **e** (red triangle symbols). **h**, Plot of t^* versus V for water droplets containing fluorescein on the reactive TiO$_2$-PVB-PDMS (blue circle symbols) and TiO$_2$-EC-PDMS (red triangle symbols) coatings (see also Supplementary Fig. 3). The lines of best fit for estimating t^* follow power law trends (as indicated by the dashed lines) of $\propto V^{1/3}$ (pre-factor = 12 min m^{-1}) for the TiO$_2$-PVB-PDMS reactive coating and $\propto V^{2/3}$ (pre-factor = 77 min m^{-2}) for the TiO$_2$-EC-PDMS reactive coating. In **f**–**h**, each data point is the average of $n = 15$ measurements (that is, five readings each for three separately prepared coating types) and the data are presented as the mean value ± standard deviation.

was repeated to create the hydrophobic photocatalytic reactive coating, but in this case the PVB binder was replaced with ethyl cellulose (EC). To demonstrate that our coatings decompose water-borne contaminants, Fig. 1c,d shows image sequences of contaminated water droplets ($V = 5\,\mu l$) that contained methyl orange at an initial concentration, C_0, of 25 ppm on the reactive TiO$_2$-PVB-PDMS and TiO$_2$-EC-PDMS coatings, respectively. We see that on the TiO$_2$-PVB-PDMS and TiO$_2$-EC-PDMS reactive coatings, the droplets change from light orange to clear after 30 and 250 min, respectively, indicating that the organic contaminants were decomposed (see also Supplementary Fig. 1c). (The total organic carbon content in the purified water samples showed comparable values to deionized water, there is no increase in the total inorganic carbon content, and no coating ingredients were detected in the purified water (Supplementary Fig. 1d–g).)

In addition, we studied the ability of the TiO$_2$-PVB-PDMS reactive coating to treat contaminants that are encountered in practice, that is, diesel[47,48] and bisphenol A[49]. Here, we irradiated a

TiO$_2$-PVB-PDMS-coated Petri dish with UV light before filling it with 100 μl of a water–diesel emulsion (initial concentration of diesel in water, $C_0 = 0.75$ ppm; see also Supplementary Fig. 2). Figure 1e shows that the concentration value of the water–diesel emulsion was reduced by 99.9% after 30 min in contact with the reactive coating. These tests were repeated for water–bisphenol A mixtures at $C_0 = 0.15$ ppm (exposure levels that are considered critical[50,51]) by dispensing 3,000 μl of the solution onto the reactive TiO$_2$-PVB-PDMS-coated Petri dish. Figure 1f shows a gradual decrease in the concentration of bisphenol A over time, and after 30 min it was no longer detectable.

Droplet purification

Epifluorescence microscopy was used to investigate the effect of the droplet volume, V, on the time taken for the reactive coatings to degrade the organic contaminant (that is, the fluorophore fluorescein) in water. We imaged the droplet–substrate interface and measured the fluorescence intensity (Fig. 2a; see Methods for image analysis details). Figure 2b

Table 1 | Coating names and compositions

Coating composition	Acronym	$\theta_a{}^*$ (°)		$\theta_r{}^*$ (°)	
		Before UV	After UV	Before UV	After UV
TiO$_2$-polyvinyl butyral-polydimethylsiloxane	TiO$_2$-PVB-PDMS	140	8	128	0
TiO$_2$-ethyl cellulose-polydimethylsiloxane	TiO$_2$-EC-PDMS	130	123	85	0

UV light exposure was 30 min for all samples. Freshly prepared (N=5) samples of each type were tested, and n=3 measurements were carried out for each sample and the mean value was taken. $\theta_a{}^*$, advancing contact angle; $\theta_r{}^*$, receding contact angle.

shows an image of the fluorescein-containing water droplet on the TiO$_2$-PVB-PDMS coating, which had not been irradiated with UV light; the droplet contact line is visible. When the coating was not activated via UV irradiation, it was hydrophobic (Table 1). To quantify the decay behaviour of the fluorophore, we selected a central area within the droplet–substrate interface and measured the mean fluorescence intensity, $\bar{I}$, as a function of time; the initial intensity value was $\bar{I}_0$. Figure 2b shows that the value of $\bar{I}/\bar{I}_0$ is relatively constant, indicating no notable change in the fluorophore concentration. Figure 2c shows a similar image sequence using the same coating, where the only difference is that the coating was irradiated with UV light for 30 min before the fluorescein water droplet was placed on it. Here, we observe that $\bar{I}/\bar{I}_0$ decreases to 0.002 within 30 min of droplet placement (see Supplementary Fig. 3a,b). We also see that we cannot identify the droplet contact line as the coating is more hydrophilic and the droplet spreads over the surface. Figure 2d,e shows similar image sequences for the TiO$_2$-EC-PDMS coating before and after UV light exposure, respectively. In both cases, we can see the droplet contact line, as the hydrophobic coating before UV activation remained so after activation with UV light (Table 1). The coating that was not exposed to UV light (Fig. 2d) showed no change in $\bar{I}/\bar{I}_0$ over time, whereas the coating that was made reactive (Fig. 2e) showed a gradual decrease in $\bar{I}/\bar{I}_0$ to a value of 0.002 at 250 min after droplet placement.

Figure 2f shows a plot of $\bar{I}/\bar{I}_0$ versus t for the cases shown in Fig. 2b,c, and Fig. 2g shows the same plot for the cases in Fig. 2d,e. In each case, the last data point that we measure is the time when $\bar{I}/\bar{I}_0$ = 0.002, and we extrapolate the profile to $\bar{I}/\bar{I}_0$ = 0.001 to find the decay time t^*. Figure 2h shows a plot of t^* versus the droplet volume V for the TiO$_2$-PVB-PDMS and TiO$_2$-EC-PDMS reactive coatings, and we see that the coating type and V have a substantial effect on t^* (see also Supplementary Fig. 3c,d). From microscopic observations, we can see that the droplet-coating contact area for the TiO$_2$-PVB-PDMS reactive coating (hydrophilic) is larger than the TiO$_2$-EC-PDMS reactive coating (hydrophobic), whereas t^* is smaller and larger for the former and latter, respectively. To understand the effect of wettability and V on t^*, we modelled the transport of the organic contaminant molecule within the droplet and reaction with the surface as a one-dimensional (z direction; with the liquid height H) diffusion–adsorption process. Once an organic contaminant molecule adsorbs to a reactive site on the surface, we assume that it is instantly degraded.

The model we used was Fick's second law:

$$\frac{\partial C}{\partial t} = -D\frac{\partial^2 C}{\partial z^2},\qquad(1)$$

with no flux and exponential decay as boundary conditions (that is, $\frac{\partial C}{\partial z}\big|_{z=H} = 0$ and $C(z=0, t) = C_0\exp^{-k_A t}$), and we assume that the adsorption process follows the Langmuir–Hinshelwood mechanism[52], where D is the diffusivity of the organic molecule in water ($D \approx 4.9 \times 10^{-6}$ cm^2 s^{-1} (ref. 53)) and k_A is the effective adsorption rate constant[52] (Supplementary Fig. 4a). The initial condition is then $C(z, t = 0) = C_0$. The value of k_A is determined experimentally and is dependent, among other things, on the ratio of organic contaminant molecules available for interaction with the number of reaction sites

present[54]. The characteristic timescales for diffusion and adsorption are given as H^2/D and $1/k_A$, respectively; the characteristic length scale is H ($\approx V/A$ for a droplet, where A is the droplet-substrate contact area), and the characteristic concentration is C_0. In the non-dimensional solution to this model, we can vary the ratio of the timescales ($k_A H^2/D$) to produce a best-fit plot with the experimental data shown in Fig. 2f,g (see Supplementary Fig. 4b,c). For a water droplet on the TiO$_2$-PVB-PDMS and TiO$_2$-EC-PDMS reactive coatings, we found that the theoretical solution best matched, respectively, the adsorption-limited ($H^2/D \ll 1/k_A$ or $k_A H^2/D = 0.00022$; $H \approx V/A = 10$ μm) and diffusion-limited ($H^2/D > 1/k_A$ or $k_A H^2/D = 3.3$; $H \approx 1.9$ mm) regimes. This means that, for the TiO$_2$-PVB-PDMS reactive coating, the time for diffusion is negligible due to the very small height, although this is the rate-limiting step in the case of the TiO$_2$-EC-PDMS reactive coating. We did further investigations with respect to different values for C_0 and H on the TiO$_2$-PVB-PDMS reactive coating using other dyes to validate the model and understand the behaviour for complete water treatment (see Supplementary Fig. 5). Increasing C_0 causes the process to be more adsorption-limited, and increasing H tends to increase the diffusion timescale. The solution pH also plays a role: contaminated water with a pH in the range of 5–10 will have a better photocatalytic effect[55], otherwise the reaction is rate reduced (Supplementary Fig. 5e).

The power law trends that we observe in Fig. 2h show that, on the TiO$_2$-PVB-PDMS reactive coating, $t^* \approx \alpha V^{1/3}$, and on the TiO$_2$-EC-PDMS reactive coating, $t^* \approx \beta V^{2/3}$: α and β are constants of proportionality. This is expected since, in the adsorption-limited regime, for a fixed C_0, t^* should increase with increasing droplet height, which for a partially wetting surface should scale as $V^{1/3}$. For the diffusion-limited regime, t^* should scale with the square of the droplet height, which for a partially wetting surface scales as $V^{2/3}$. In the adsorption-limited regime, t^* should decrease for increasing numbers of reactive sites on the surface, which we also investigated. We found that we were at the maximum surface reactivity that can be achieved by increasing the TiO$_2$ nanoparticle concentration (see Supplementary Fig 6).

Fog harvesting and purification

The laboratory-scale fogging setup shown in Fig. 3a was used to study the real-time water harvesting and treatment performance of the coated meshes. The fog, which contained the methyl orange contaminant, was injected at a velocity v_{fog} into the tunnel, at the end of which was the mesh. The fog velocity can vary from 1 to 8 m s^{-1} depending on the application[19], and we chose $v_{fog} = 1.5$ m s^{-1} since this is the lower end of the fog speed range, which is where it is most contaminated[56]. The mass flux of fog $4\dot{m}/(\pi\Phi^2)$ (-0.036 g cm^{-2} min^{-1}) represents standard fog harvesting conditions[19], which is higher compared with other laboratory-scale setups, where $\dot{m}$ is the fog mass flow rate and Φ is the fog tunnel diameter. Once the fog had been captured on the mesh, it drained into a collector below, which was attached to a balance that we used to measure the mass of the collected water m_c (see Supplementary Fig. 7a–c). Each experiment lasted $\Delta t \approx 66$ min, and afterwards the concentration of the pollutants in the collected water, C, was measured. By comparing C_0 and C we can calculate the water treatment efficiency $(1 - C/C_0)$. We can also calculate the fog harvesting efficiency as $m_c/(\dot{m}\Delta t)$.
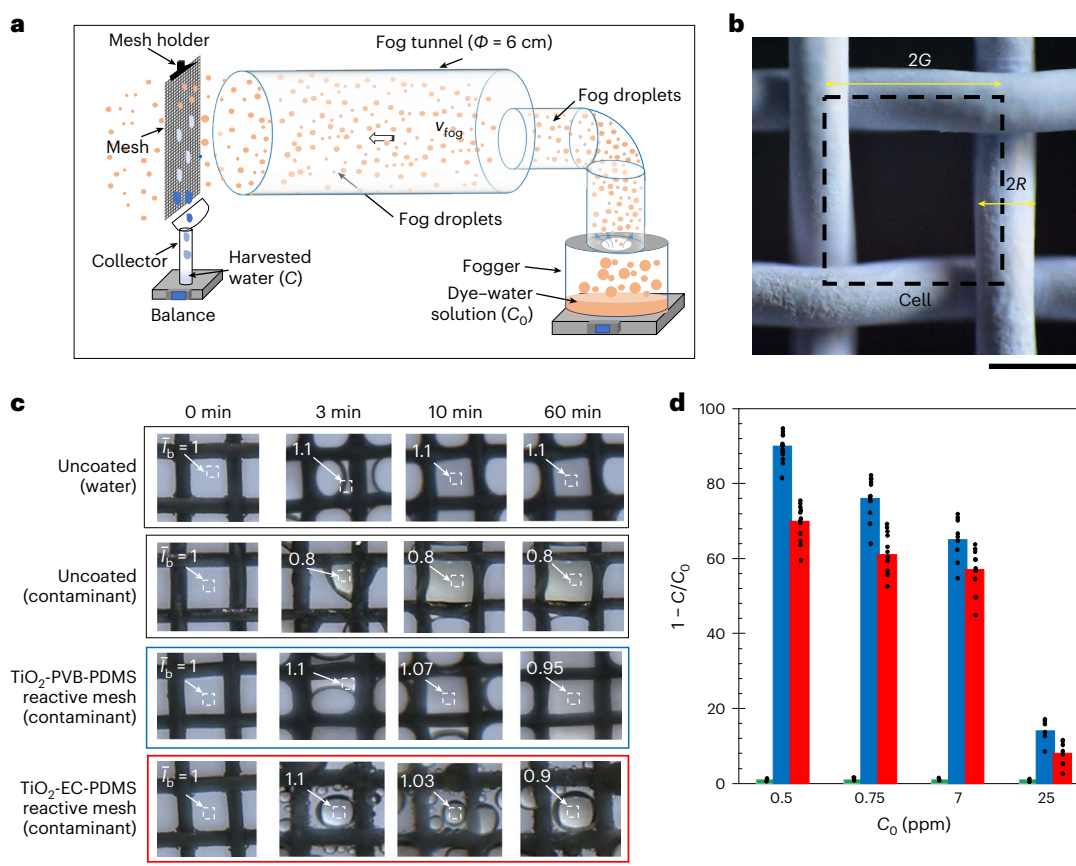
Fig. 3 | Harvesting and treating contaminated fog with nanoengineered reactive meshes. a, Schematic showing the laboratory-scale fog harvesting setup used to generate contaminated fog (containing methyl orange) at an initial concentration C_0, along with the fog harvesting and treatment, and measurement of the final concentration (C) of methyl orange. Φ, is the fog tunnel diameter. **b**, Micrograph showing a single unit cell of the mesh (stainless steel), where R is the radius of the mesh wire and $2G$ is the wire spacing. Scale bar, 0.4 mm. **c**, Colour image sequence showing the mesh surfaces during fog harvesting experiments in the presence ($C_0 = 25$ ppm) and absence ($C_0 = 0$ ppm) of contaminated fog. The control experiments used uncoated meshes, and the reactive coatings TiO$_2$-PVB-PDMS and TiO$_2$-EC-PDMS were used after UV irradiation. The dashed white box indicates the region where the intensity of the colour blue, $\bar{I}_b$, was measured (aqueous methyl orange absorbs blue light[57]); the box location varies since the droplet–mesh interaction is different in each case. Before the fogging starts, the value of $\bar{I}_b$ for the window is normalized and set to unity. Scale bar, 0.4 mm. **d**, Quantifying the effect of C_0 on the ability of the mesh coating to treat the intercepted fog: uncoated mesh (green bar), TiO$_2$-PVB-PDMS reactive mesh (blue bar) and TiO$_2$-EC-PDMS reactive mesh (red bar). The bar represents the mean value for $n = 15$ experiments and the data distribution is shown by the black dots. C was measured at $t = 66$ min; fog harvesting experiments were started at $t = 0$ min. For all runs, the fog velocity was kept constant ($v_{fog} = 1.5$ m s^{-1}).

Figure 3b shows a single cell of the mesh, where $R = 125$ μm is the radius of the mesh wire and $2G = 600$ μm is the spacing between two adjacent wires (this mesh design lies within the optimum collection regime[23]). Figure 3c (top row) shows an image sequence of the fog droplets collected using this mesh type with no coating treatment and for fog generated from water that contained no methyl orange ($C_0 = 0$). The next rows show intercepted droplets from fog that initially contained methyl orange ($C_0 = 25$ ppm) using the same mesh with no coating treatment (second row), using the TiO$_2$-PVB-PDMS-coated mesh (third row) and using the TiO$_2$-EC-PDMS-coated mesh (fourth row). We see that the fog that collects on the uncoated mesh surface is clear when it is uncontaminated and yellowish when it is contaminated. For the reactive coated meshes, the contaminated water droplets appear clear at the beginning but over time become slightly yellowish, qualitatively indicating a drop in the water treatment performance. In the droplets between the mesh wires we measured the intensity of the colour blue ($\bar{I}_b$) since aqueous methyl orange absorbs blue light[57]—to quantify the change relative to before any droplets were collected. In Fig. 3d we quantify the effect of C_0 in the fog on the performance of the control and the two reactive coatings in terms of $(1 - C/C_0)$. We observed that the uncoated mesh, the TiO$_2$-PVB-PDMS reactive coating and the TiO$_2$-EC-PDMS reactive coating have a fog harvesting efficiency of $m_c/(\dot{m}\Delta t) = 5.6\%$, 8.0% and 3.8%, respectively. From this we see that the TiO$_2$-PVB-PDMS reactive coating is ~50% better than the TiO$_2$-EC-PDMS reactive coating for directly harvesting fog, consistent with previous reports[24] where surfaces with lower contact angle hysteresis and lower receding contact angles are superior (Supplementary Fig. 7e). The concentration of $C_0 = 0.5$ ppm, which is the maximum allowable limit for the most abundantly available airborne organic contaminants[58], has a $(1 - C/C_0)$ value of 91% for the TiO$_2$-PVB-PDMS-coated reactive mesh, and 14% at the higher methyl orange concentration of $C_0 = 25$ ppm. (Supplementary Figure 7f shows a study of control experimental cases to confirm that the treatment efficiency considered is due only to the reactive reduction in contaminant concentration and is not influenced by surface adsorption.) We performed a total organic carbon content analysis for the contaminated water before and after fog harvesting and treatment to calculate the true extent of organic molecule decay. The reduction in the total organic carbon content was 60% and 12%, respectively, for $C_0 = 7$ and 25 ppm on the reactive TiO$_2$-PVB-PDMS-coated mesh (Supplementary Fig. 7g). This is consistent with our results using
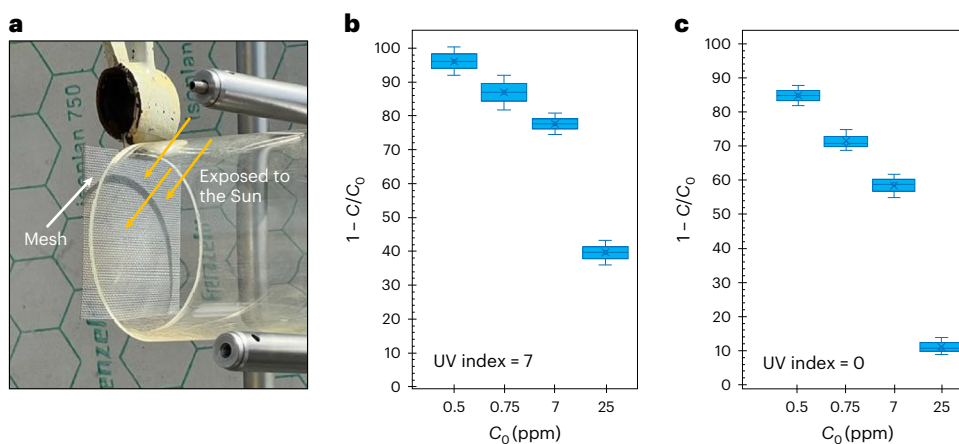
Fig. 4 | Outdoor demonstration of fog harvesting and treatment on sunny and cloudy days. a, Image of the TiO$_2$-PVB-PDMS reactive mesh and fog tunnel setup placed on the roof of the 'ML' building at ETH Zurich, Switzerland (latitude 47.38° N, longitude 8.55° E). **b**, The decay efficiency for the dye solution during the month of July in 2022 when the UV index was 7 (which denotes high UV exposure from the Sun) and the outdoor temperature ranged between 25 °C and 33 °C, using the setup shown in **a** for various initial concentrations of methyl orange in the fog water. **c**, The decay efficiency during the month of January in 2023 on a cloudy day when the UV index was ~0 (denoting low UV exposure from

the Sun) and the temperature varied between 8 °C and 9 °C, using the setup shown in **a** for various initial concentrations of methyl orange in the fog water. Here the coated mesh was pre-activated with UV irradiation before it was used in the outdoor experiments. In the box plots of **b** and **c**, the centre line denotes the mean value, the box bounds indicate the 25th/75th percentile values and the whiskers indicate the minimum/maximum values. For each box the sample size was $n = 15$ (five readings each for three separately prepared coated meshes) for the experiments.

UV-vis spectroscopy where we found that $(1 − C/C_0) = 65\%$ for $C_0 = 7$ ppm and 14% for $C_0 = 25$ ppm (Fig. 3d).

It is instructive to compare our fog harvesting and water treatment results with single-droplet experiments ($C_0 = 25$ ppm), particularly for V and t^* against the thickness of the water film on the mesh (h) and the water–substrate residence time (t_r). Using the conservation of mass and assuming quasi-steady-state behaviour, we can estimate t_r for a mesh of width (W) and thickness ($2R$) by dividing half the length of the mesh ($L/2$) by the average water-drainage velocity ($\dot{m}_c/(2RW\rho)$):

$$t_r = LRW\rho/\dot{m}_c, \qquad (2)$$

where $\dot{m}_c$ is the collected fog mass flow rate and ρ is liquid density. Substituting appropriate values (that is, $\rho = 1.0$ g cm^{-3}, $W = 6.0$ cm, $L = 6.0$ cm, $R = 0.0125$ cm, $\dot{m}_c = 0.023$ g min^{-1}) yields $t_r = 20$ min (see Supplementary Fig. 7e). Owing to the different wettability characteristics of the reactive meshes, we found that the intercepted fog droplets on the TiO$_2$-EC-PDMS reactive mesh formed discrete growing droplets that could be visualized and characterized, whereas for the TiO$_2$-PVB-PDMS reactive mesh the intercepted droplets formed a more film-like layer, making comparison with the earlier single-droplet experiments more challenging. On the TiO$_2$-EC-PDMS reactive surface (hydrophobic), the droplets depart the mesh surface when two droplets coalesce, and the volume of one of these pre-coalescence droplets is typically ~0.3 μl (Supplementary Fig. 7c). During the early stages of growth, where the droplet radius is $<R$, the wetting behaviour resembles a droplet on a relatively flat substrate (compare Fig. 2), whereas for the late stages of growth, where the droplet diameter is ~$2(G + R)$, the contact with the reactive surface area is reduced compared with the droplet volume and decay is expected to be slower than for the droplet case. We make the conservative assumption that the growing droplets have reactive-surface-area-to-liquid-volume ratios (that is, A/V) that are similar to the mesh wire, which is similar to the earlier single-droplet experiments on flat TiO$_2$-EC-PDMS reactive coatings, and from this we find that $t^* \approx 36$ min (see Fig. 2h; $V = 0.3$ μl, $C_0 = 25$ ppm). By defining the ratio t_r/t^*, we can roughly estimate how close we are to complete water treatment ($C_0 = 25$ ppm), which here is 0.56. We can contrast that

with the measured experimental results of $(1 − C/C_0) = 11\%$ (Fig. 3d), and we see that the ration of the residence time to the treatment time is of the same order of magnitude as the water treatment efficiency, supporting our claims. We note here that our choice of the mass flux of fog is relatively high, at ~0.036 g cm^{-2} min^{-1} compared with previous fog studies where it ranged up to 0.025 g cm^{-2} min^{-1} or less[15,24], and we expect that the residence time will increase for such applications, thereby increasing $(1 − C/C_0)$ for higher contaminant concentrations. Moreover, ultrafast transport of droplets from the surface to the collector is not ideal for our application since the residence time of the droplet is important for the water treatment efficiency. Thus, we find that the engineered hydrophilic surface outperforms the hydrophobic surface in both collection and treatment efficiencies.

Outdoor experiments

The previous experiments were all conducted using coated meshes that were pre-activated using UV irradiation. However, in real applications, it may be the case that the meshes can also receive some amount of sunlight exposure (Fig. 4a). Thus we performed outdoor tests, using the same experimental setup as was used in the laboratory, on the roof of a building at ETH Zurich, Switzerland (latitude 47.38° N, longitude 8.55° E) during 25–29 July 2022 between 10:00 and 16:00 (UTC + 02:00) at outdoor temperatures of 25–33 °C, where the UV index of the solar radiation was 7 (a value of >10 denotes extreme conditions (data taken from MeteoSwiss); see also Supplementary Fig. 7d). Figure 4b shows a plot of $(1 − C/C_0)$ versus C_0 for the TiO$_2$-PVB-PDMS-coated reactive mesh, the best performing coating from the laboratory experiments, where $(1 − C/C_0)$ varies between 94% and 39% for C_0 between 0.5 ppm and 25 ppm, respectively. The improved water treatment efficiency values in the outdoor tests are due to continuous activation of the reactive coating by the Sun. The same outdoor experiments were repeated on cloudy days (UV index ≈ 0, on 10–14 January 2023 and 24–28 January 2023) using a TiO$_2$-PVB-PDMS-coated mesh that was pre-activated with UV irradiation. These results (Fig. 4c) show a similar trend to the outdoor experiments when the UV index is high—albeit with a lower performance—as well as being similar to the indoor laboratory experiments (Fig. 3).

Discussion

We demonstrated a fully passive fog harvesting and water treatment system that is capable of capturing fog at high efficiency while simultaneously removing organic contaminants in an energy-neutral way. The system consists of a fog harvesting mesh with a solar-light-activated reactive coating, whose wettability can be tuned and remains reactive even in the absence of UV light, for example, on a cloudy day, enabling us to rationally engineer it to achieve a high level of fog harvesting with short contaminant-removal times. Using epifluorescence microscopy, we explore the effect of wettability and droplet volume with respect to the time it takes to degrade contaminants in a single droplet, and explain the results obtained using a diffusion–adsorption–reaction model, with the hydrophobic and hydrophilic reactive coatings being in diffusion- and adsorption-limiting regimes, respectively. By embedding photocatalytic nanoparticles in the reactive coatings at the maximum concentration—while maintaining good coating adhesion—we ensured a high number of reactive sites and minimal water treatment times. When deposited onto a mesh substrate, we found that the TiO_2-PVB-PDMS reactive coating was better for harvesting and water treatment efficiencies compared with the TiO_2-EC-PDMS reactive coating. We attribute the better water treatment performance of TiO_2-PVB-PDMS to the lower droplet contact angles and therefore shorter contaminant diffusion length compared with TiO_2-EC-PDMS, which is supported by high-speed imaging as well as experimental and theoretical treatment-time results. We then performed outdoor tests, where the water treatment efficiency of the TiO_2-PVB-PDMS reactive mesh was over 90% under high UV index conditions and a respectable 85% when the UV index was zero. Such a performance at these concentrations is notable since the maximum allowable limit for the most abundantly available airborne organic contaminants is 0.5 ppm, thereby demonstrating the promise of this technology. Thus, our study shows promise towards the development of water harvesting systems with passive water purification properties, in this case harnessing intermittent solar resources to harvest and treat water on foggy days, providing a pathway towards creating potable water from underutilized water sources and addressing the global challenge of water scarcity.

Methods

Materials and reagents

Glass slides (Avantor, VWR) and stainless steel meshes (grade SS 304; Drahtgewebe-Shop) were used as the coating substrates. The meshes were corrosion-resistant and had a wire diameter of $2R = 0.25$ mm, a wire spacing of $2G = 0.6$ mm and a single-layer orthogonal grid weave. We selected the mesh by considering the recommendations on mesh structural parameters for achieving an optimum mesh–droplet interaction to enhance the fog harvesting yield[23]. TiO_2 nanopowder (Aeroxide P25; 77.1% anatase, 15.9% rutile) was acquired from Acros Organics. PVB ($M_w = 50$–80 kDa), EC (48.0–49.5% w/w ethoxyl basis), dichlorodimethylsilane (≥98.5% GC), toluene (≥99.7% GC), methyl orange (ACS reagent, dye content 85%) and fluorescein sodium salt were purchased from Sigma-Aldrich. 4,4′-Isopropylidenediphenol (bisphenol A; 97%) was purchased from Thermo Fisher Scientific. All chemicals were used without further purification. Methyl orange is an organic molecule of the azo dye family, which causes water pollution and irrevocable environmental problems[59], and has distinct colour variations even at very low concentrations, making it a suitable surrogate contaminant. Fluorescein sodium salt has a similar molecular weight to methyl orange and the necessary fluorescence properties for epifluorescence studies. Diesel was taken from a regular vehicle filling station. An ultrasonic humidifier (Maxi Fogger; with a fogging generation rate of up to 500 ml h^{-1}) was used to generate the artificial fog. Although it is possible to carry out fog harvesting studies with natural fog[9,21], this was not suitable for our fundamental investigation and thus we opted to generate artificial fog for the purposes of studying the fog collection and water treatment efficiency. The fog was guided using a custom-made transparent acrylic tube (diameter = 6 cm, length = 15 cm; see Fig. 3a). The flow velocity was measured using an anemometer (UNI-T; with a precision of 0.1 m s^{-1}). For outdoor experiments the dye solution used to generate the contaminated fog was kept in the dark to stop self-degradation due to sunlight exposure[46].

Surface preparation

The glass slides (7.5×2.5 cm^2) and the metal meshes (6×6 cm^2) were cleaned with acetone and then with isopropanol using an ultrasonicating water bath (Branson 2800) before being rinsed thoroughly with deionized water and drying with nitrogen. The TiO_2 nanoparticles (0.02 g ml^{-1}) were added to ethanol and sonicated using a bath sonicator for one hour to produce a homogeneous suspension. Two separate coating dispersions were prepared by adding either PVB or EC (0.001 g ml^{-1}) as the binder to the suspension under continuous stirring using a magnetic stirrer for 30 min. The binder provides mechanical stability to the coating by enhancing its adhesion to the substrate. The dispersions were then sprayed onto the substrates (using an air pressure of 3 bar) using a double-action, internal-mix, siphon-feed airbrush (VL series, Paasche) from a distance of ~20 cm. The glass substrates were coated on one side, and the metal meshes were coated on both sides. The coated surfaces were dried inside an oven (BINDER) at 60 °C for one hour (Supplementary Fig. 8a). Normally, such coatings become superhydrophilic when they are irradiated with UV light[60], but there is evidence of making them less hydrophilic in a stable way via grafting a PDMS brush on the metal oxides[61,62]. To graft the silicone brush onto the TiO_2 nanoparticles, the freshly coated surfaces were treated with oxygen plasma (Femto, Diener Electronic) for 3 min at 100 W to achieve surface activation. Then they were placed in a bath containing a 30:1 (v/v) ratio of, respectively, toluene mixture and dichlorodimethylsilane (the organic silicon monomer of PDMS) for 30 min at room temperature to form the brush layer, which regulates the coating wettability (Table 1) and promotes substrate adhesion (Supplementary Fig. 8b,c). Toluene mixtures were prepared by adding water to toluene in the ratio of 5:1 (v/v), respectively, while using a magnetic stirrer plate. The mixture was then left to stabilize for one day. The silicon-brush-grafted surfaces were washed with copious amounts of toluene and deionized water to remove any residual silane constituents.

The surfaces were then put under a UV light exposure unit (Proma) with an intensity of 165 W m^{-2} and an emitting wavelength of 365 nm for 30 min for photocatalytic activation. It was seen that 30 min of exposure to the Sun adequately activates the photocatalytic surface[46]; thus; the present UV lamp, which emits threefold higher radiation compared with the Sun, provides adequate activation. This coating becomes photocatalytically active and therefore reactive upon exposure to UV light or sunlight, and at the same time it becomes superhydrophilic when the binder is PVB but hydrophobic when the binder is EC (Supplementary Fig. 8e,f). We know from previous literature[45] that the change in wettability and reactivity are both attributed to the formation of electron–hole pairs, and thus the retention of the modified surface wettability indicates the existence of electron–hole pairs as well as the surface reactivity. The mechanism of why the different binders cause the reactive surfaces to exhibit different wettability characteristics was investigated, and we found that the composition of the grafted brush layer is different for each binder. When EC is the binder, the brush layer reacts fully to become PDMS. When PVB is the binder, the brush layer—after exposure to water—contains chlorine in substantial quantities, indicating that the PDMS has not reacted fully (see Supplementary Table 1 for energy-dispersive X-ray spectroscopy analysis). To demonstrate that the substrates were indeed coated with a stable PDMS layer, we carried out X-ray photoelectron spectroscopy analysis. The Si–O peak on the PDMS-coated surfaces in both the freshly prepared and used samples (for cleaning the contaminated water) was prominent, whereas a negligible quantity was observed in the non-PDMS-coated surfaces, confirming the stability of the PDMS brush (Supplementary Fig. 9).

Characterization

In all of our laboratory experiments, the engineered coatings were pre-activated via UV irradiation for 30 min, which were termed 'reactive' coatings, and then the experiments were carried out in the absence of UV light. The efficacy of the organic contaminant (dye) decay was explored in two ways. First, droplets containing the florescent dye fluorescein (excitation wavelength 465–490 nm (ref. 63)) were imaged using an epifluorescence microscope (Eclipse Ti2 inverted microscope, Nikon) using a ×10 objective. The droplets on the reactive coatings were covered with small chambers proportional to their size to minimize evaporation. Then a light source (a light-emitting diode with an emission wavelength of 470 nm) was used to excite the dye molecules and images were obtained (using a Hamamatsu scientific CMOS camera) at periodic intervals until the florescence was no longer visible, indicating the complete decay of the dye molecules. When the fluorescent droplet was placed on the coating it had a fluorescence intensity at time $t = 0$ (Fig. 2b–e), and this intensity was retained if the coating was not reactive (Fig. 2b,d, at $t = 30$ and 250 min, respectively) but faded if the surface was reactive (Fig. 2c,e, at $t = 30$ and 250 min, respectively). By measuring and analysing the fluorescence intensity of the images (using the ImageJ software), a plot of intensity versus time (I–t) can be generated (Supplementary Fig. 3). Considering the known initial concentration of the contaminant (C_0) in the deposited droplet and equating it with the initial mean intensity ($\bar{I}_0$), the dye concentration at any time ($C(t)$) can be measured from the intensity plot and hence the decay behaviour can be determined (Supplementary Fig. 3). It was confirmed that the microscope excitation light did not have any effect on the decay of the fluorescent molecules (Fig. 2b–d).

Second, the fogging setup was built to carry out indoor laboratory-scale and outdoor fog experiments. The contaminant concentration in the collected water from the fog harvesting mesh was analysed via absorbance spectroscopy using a UV-vis spectrophotometer (Jasco V-770). To confirm the stability of the coating after repeated exposure to UV radiation—both mechanically as well as for water treatment—we analysed the coating integrity microscopically and measured the decay efficiency using the same TiO_2-PVB-PDMS-coated reactive mesh for multiple runs (Supplementary Fig. 8d). We also performed X-ray photoelectron spectroscopy on the TiO_2-PVB-PDMS coating before and after UV radiation and water treatment, and found no degradation of the PDMS brush layer (Supplementary Fig. 9). The deposition and growth of the fog droplet on the mesh wire was studied using a high-speed camera (Photron SA1.1) at 250 frames per second. Mettler Toledo balances (with precision values of 0.1 mg and 1 g) were used for weighing the chemicals, fogging rate and collected water. Optical micrographs of the coatings were obtained using an Olympus BX60 microscope with an Olympus SC-50 microscope camera. Contact angle measurements were carried out by dispensing deionized water droplets onto the surface of a goniometer (TBU 90E, DataPhysics). In addition, electron micrographs showing the coating-surface textures were obtained via scanning electron microscopy (SU8230, Hitachi). Energy-dispersive spectroscopy was also carried out using the same setup. Fogging on the mesh was imaged using a colour CCD (charge-coupled device) camera (FLIR Integrated Imaging Solutions). The water quality was tested (Supplementary Fig. 1) using inductively coupled plasma optical emission spectroscopy (5100 VDV, Agilent) and a total organic carbon analyser (TOC-V, Shimadzu). Inductively coupled plasma optical emission spectroscopy helps in detecting any traces of Ti and Si in the treated water, whereas the total organic carbon analyser catalytically oxidizes the treated water sample at a high temperature (~720 °C) and converts the organic carbon in the solution into CO_2. The CO_2 generated is measured to estimate the total organic carbon content of the sample.

For the experiments using the water–diesel mixture, the concentration of diesel was 0.75 ppm. The concentration chosen here for our experiments was matched with the permissible exposure level of formaldehyde, which is the most common environmental contaminant emitted from the combustion of diesel[64], and 0.75 ppm is the maximum permissible exposure level of formaldehyde[58] that is allowed by the US Occupational Safety and Health Administration. As diesel and water are immiscible, the deionized water was first degassed and then an adequate amount of diesel was added to it. The mixture was then ultrasonicated for two hours in a bath to obtain a stable suspension of diesel droplets. UV-vis spectroscopy was used to compare the absorbance between treated and untreated water–diesel emulsions (Supplementary Fig. 2). Similarly, for experiments with bisphenol A, $C_0 = 0.15$ ppm in water was considered for our experiments, in line with previous literature reports referring to various exposure levels that are critical in the environment. High-performance liquid chromatography (1200 Series, Agilent Technologies; using a 220 nm photodiode array detection intensity) was used to compare the treated and untreated water samples.

Reporting summary

Further information on research design is available in the Nature Portfolio Reporting Summary linked to this article.

Data availability

All data needed to evaluate the conclusions in the paper are present in the paper and/or the Supplementary Information. All other source data are available in the ETH Zurich Research Collection at https://doi.org/10.3929/ethz-b-000608600.

References

1. Mekonnen, M. M. & Hoekstra, A. Y. Four billion people facing severe water scarcity. *Sci. Adv.* **2**, e1500323 (2016).
2. Gleeson, T., Wada, Y., Bierkens, M. F. P. & van Beek, L. P. H. Water balance of global aquifers revealed by groundwater footprint. *Nature* **488**, 197–200 (2012).
3. Smalley, R. E. Future global energy prosperity: the terawatt challenge. *MRS Bull.* **30**, 412–417 (2005).
4. Ali, K. et al. Characterization and source identification of $PM_{2.5}$ and its chemical and carbonaceous during Winter Fog Experiment 2015–16 at Indira Gandhi International Airport, Delhi. *Sci. Total Environ.* **662**, 687–696 (2019).
5. Wang, W. et al. Chemical compositions of fog and precipitation at Sejila Mountain in the southeast Tibetan Plateau, China. *Environ. Pollut.* **253**, 560–568 (2019).
6. Rockström, J. & Falkenmark, M. Agriculture: Increase water harvesting in Africa. *Nature* **519**, 283–285 (2015).
7. Schemenauer, R. S. & Cereceda, P. Fog-water collection in arid coastal locations. *Ambio* **20**, 303–308 (1991).
8. Ghosh, R. & Ganguly, R. Harvesting Water from Natural and Industrial Fogs—Opportunities and Challenges in *Droplet and Spray Transport: Paradigms and Applications* (eds Basu, S. et al.) 237–266 (Springer, 2018).
9. Jaén, M. V. M. Fog water collection in a rural park in the Canary Islands (Spain). *Atmos. Res.* **64**, 239–250 (2002).
10. Haechler, I. et al. Exploiting radiative cooling for uninterrupted 24-hour water harvesting from the atmosphere. *Sci. Adv.* **7**, eabf3978 (2021).
11. Lord, J. et al. Global potential for harvesting drinking water from air using solar energy. *Nature* **598**, 611–617 (2021).
12. Kim, H. et al. Adsorption-based atmospheric water harvesting device for arid climates. *Nat. Commun.* **9**, 1191 (2018).
13. Wang, Y. et al. Heterogeneous wettability and radiative cooling for efficient deliquescent sorbents-based atmospheric water harvesting. *Cell Rep. Phys. Sci.* **3**, 100879 (2022).
14. Ghosh, R., Ray, T. K. & Ganguly, R. Cooling tower fog harvesting in power plants – a pilot study. *Energy* **89**, 1018–1028 (2015).
15. Damak, M. & Varanasi, K. Electrostatically driven fog collection using space charge injection. *Sci. Adv.* **4**, eaao5323 (2018).

16. Wimalawansa, S. J. Purification of contaminated water with reverse osmosis: effective solution of providing clean water for human needs in developing countries. *Int. J. Emerg. Technol. Adv. Eng.* **3**, 75–89 (2013).

17. UNESCO World Water Assessment Programme *The United Nations World Water Development Report 2014: Water and Energy* (UNESCO, 2014).

18. UNESCO World Water Assessment Programme *The United Nations World Water Development Report 2020: Water and Climate Change* (UNESCO, 2020).

19. Schemenauer, R. S., Cereceda, P. & Osses, P. *Fog Water Collection Manual* (FogQuest, 2022).

20. Thalmann, E., Burkard, R., Wrzesinsky, T., Eugster, W. & Klemm, O. Ion fluxes from fog and rain to an agricultural and a forest ecosystem in Europe. *Atmos. Res.* **64**, 147–158 (2002).

21. Shi, W., van der Sloot, T. W., Hart, B. J., Kennedy, B. S. & Boreyko, J. B. Harps enable water harvesting under light fog conditions. *Adv. Sustain. Syst.* **4**, 2000040 (2020).

22. Mazoyer, M., Burnet, F. & Denjean, C. Experimental study on the evolution of droplet size distribution during the fog life cycle. *Atmos. Chem. Phys.* **22**, 11305–11321 (2022).

23. Rivera, J. D. Aerodynamic collection efficiency of fog water collectors. *Atmos. Res.* **102**, 335–342 (2011).

24. Park, K. C., Chhatre, S. S., Srinivasan, S., Cohen, R. E. & McKinley, G. H. Optimal design of permeable fiber network structures for fog harvesting. *Langmuir* **29**, 13269–13277 (2013).

25. Shanyengana, E. S., Sanderson, R. D., Seely, M. K. & Schemenauer, R. S. Testing greenhouse shade nets for the collection of fog for use as a water supply. *J. Water Supply Res. Technol. Aqua* **52**, 237–241 (2003).

26. Li, J. et al. Aerodynamics-assisted, efficient, and scalable *kirigami* fog collectors. *Nat. Commun.* **12**, 5484 (2021).

27. Rivera, J. D. & Lopez-Garcia, D. Mechanical characteristics of Raschel mesh and their application to the design of large fog collectors. *Atmos. Res.* **151**, 250–258 (2015).

28. Holmes, R., Rivera, J. D. & de la Jara, E. Large fog collectors: new strategies for collection efficiency and structural response to wind pressure. *Atmos. Res.* **151**, 236–249 (2015).

29. Azad, M. A. K., Ellerbrok, D., Barthlott, W. & Koch, K. Fog collecting biomimetic surfaces: influence of microstructure and wettability. *Bioinspir. Biomim.* **10**, 016004 (2015).

30. Ju, J., Xiao, K., Yao, X., Bai, H. & Jiang, L. Bioinspired conical copper wire with gradient wettability for continuous and efficient fog collection. *Adv. Mater.* **25**, 5937–5942 (2013).

31. Zheng, Y. et al. Directional water collection on wetted spider silk. *Nature* **463**, 640–643 (2010).

32. Yang, X., Song, J., Liu, J., Liu, X. & Jin, Z. A twice electrochemical-etching method to fabricate superhydrophobic–superhydrophilic patterns for biomimetic fog harvest. *Sci. Rep.* **7**, 8816 (2018).

33. Zhong, L., Feng, J. & Guo, Z. An alternating nanoscale (hydrophilic–hydrophobic)/hydrophilic Janus cooperative copper mesh fabricated by a simple liquidus modification for efficient fog harvesting. *J. Mater. Chem. A* **7**, 8405–8413 (2019).

34. Feng, S. et al. Tip-induced flipping of droplets on Janus pillars: from local reconfiguration to global transport. *Sci. Adv.* **6**, eabb4540 (2020).

35. Feng, S. et al. Three-dimensional capillary ratchet-induced liquid directional steering. *Science* **373**, 1344–1348 (2021).

36. Yadav, R. & Pandey, P. A review on volatile organic compounds (VOCs) as environmental pollutants: fate and distribution. *Int. J. Plant Environ.* **4**, 14–26 (2018).

37. Capel, P. D., Leuenberger, C. & Giger, W. Hydrophobic organic chemicals in urban fog. *Atmos. Environ. A* **25**, 1335–1346 (1991).

38. Waldman, J. M. et al. Chemical composition of acid fog. *Science* **218**, 677–680 (1982).

39. Yu, L. et al. The degradation mechanism of methyl orange under photo-catalysis of TiO_2. *Phys. Chem. Chem. Phys.* **14**, 3589–3595 (2012).

40. Chen, Y. et al. Selective recovery of precious metals through photocatalysis. *Nat. Sustain.* **4**, 618–626 (2021).

41. Khalilova, H. K., Hasanova, S. A. & Aliyev, F. G. Photocatalytic removal of organic pollutants from industrial wastewater using TiO_2 catalyst. *J. Environ. Prot.* **9**, 691–698 (2018).

42. Zahid, M. et al. Fabrication of visible light-induced antibacterial and self-cleaning cotton fabrics using manganese doped TiO_2 nanoparticles. *ACS Appl. Bio Mater.* **1**, 1154–1164 (2018).

43. Nakano, R. et al. Inactivation of various variant types of SARS-CoV-2 by indoor-light-sensitive TiO_2-based photocatalyst. *Sci. Rep.* **12**, 5804 (2022).

44. Mahapatra, P. S., Chatterjee, S., Tiwari, M. K., Ganguly, R. & Megaridis, C. M. Surface treatments to enhance the functionality of PPEs. *Trans. Indian Natl Acad. Eng.* **5**, 333–336 (2020).

45. Fujishima, A., Hashimoto, K. & Watanabe, T. *TiO_2 Photocatalysis: Fundamentals and Applications* (BKC, 1999).

46. Ghosh, R., Sahu, R. P., Ganguly, R., Zhitomirsky, I. & Puri, I. K. Photocatalytic activity of electrophoretically deposited TiO_2 and ZnO nanoparticles on fog harvesting meshes. *Ceram. Int.* **46**, 3777–3785 (2020).

47. Breeze, P. in *Electricity Generation and the Environment* 33–47 (Academic, 2017).

48. Janarthanan, K. & Sivanandi, P. Extraction and characterization of waste plastic pyrolysis oil for diesel engines. *J. Clean. Prod.* **366**, 132924 (2022).

49. La Merrill, M. A. et al. Consensus on the key characteristics of endocrine-disrupting chemicals as a basis for hazard identification. *Nat. Rev. Endocrinol.* **16**, 45–57 (2020).

50. Canesi, L. & Fabbri, E. Environmental effects of BPA: focus on aquatic species. *Dose Response* https://doi.org/10.1177/1559325815598304 (2015).

51. Fonseca, M. I., Lorigo, M. & Cairrao, E. Endocrine-disrupting effects of bisphenol A on the cardiovascular system: a review. *J. Xenobiot.* **12**, 181–213 (2022).

52. Ohtani, B. in *Advances in Inorganic Chemistry* Vol. 63 (eds van Eldik, R. & Stochel, G.) Ch. 10 (Academic, 2011).

53. Rani, S. A., Pitts, B. & Stewart, P. S. Rapid diffusion of fluorescent tracers into Staphylococcus epidermidis biofilms visualized by time lapse microscopy. *Antimicrob. Agents Chemother.* **49**, 728–732 (2005).

54. Li, Y., Li, X., Li, J. & Yin, J. Photocatalytic degradation of methyl orange by TiO_2-coated activated carbon and kinetic study. *Water Res.* **40**, 1119–1126 (2006).

55. Reza, K. M., Kurny, A. S. W. & Gulshan, F. Parameters affecting the photocatalytic degradation of dyes using TiO_2: a review. *Appl. Water Sci.* **7**, 1569–1578 (2017).

56. Kim, K. H., Lee, S., Woo, D. & Bae, G. Influence of wind direction and speed on the transport of particle-bound PAHs in a roadway environment. *Atmos. Pollut. Res.* **6**, 1024–1034 (2015).

57. Ocholi, O. J. et al. Effect of time on the adsorption of methylene blue, methyl orange and indigo carmine onto activated carbon. *IOSR J. Appl. Chem.* **9**, 55–62 (2016).

58. *Table AC-1: Permissible Exposure Limits for Chemical Contaminants* Chemical Abstracts Registry Number 50000 (California Division of Occupational Safety and Health, accessed 20 July 2022); https://www.dir.ca.gov/title8/5155table_ac1.html

59. Kalme, S. D., Parshetti, G. K., Jadhav, S. U. & Govindwar, S. P. Biodegradation of benzidine based dye Direct Blue-6 by *Pseudomonas desmolyticum* NCIM 2112. *Bioresour. Technol.* **98**, 1405–1410 (2007).

60. Sun, R. D., Nakajima, A., Fujishima, A., Watanabe, T. & Hashimoto, K. Photoinduced surface wettability conversion of ZnO and TiO₂ thin films. *J. Phys. Chem. B* **105**, 1984–1990 (2001).

61. Wooh, S., Encinas, N., Vollmer, D. & Butt, H.-J. Stable hydrophobic metal-oxide photocatalysts via grafting polydimethylsiloxane brush. *Adv. Mater.* **29**, 1604637 (2017).

62. Liu, J. et al. Optimizing hydrophobicity and photocatalytic activity of PDMS-coated titanium dioxide. *ACS Appl. Mater. Interfaces* **11**, 27422–27425 (2019).

63. Olson, J. L. & Mandava, N. Fluorescein Angiography in *Retinal Imaging* (eds Huang, D. et al.) Ch. 1 (Elsevier, 2006).

64. Salonen, H. et al. Volatile organic compounds and formaldehyde as explaining factors for sensory irritation in office environments. *J. Occup. Environ. Hyg.* **6**, 239–247 (2009).

Acknowledgements

Author contributions

R.G. and T.M.S. designed the study. R.G., M.K., H.-J.B. and T.M.S. provided scientific guidance throughout. R.G., A.B. and G.B. conducted the experiments. R.G., A.B., G.B. and T.M.S. performed the theoretical modelling. R.G. synthesized and characterized the samples. R.G. and M.K. analysed the data. R.G. and T.M.S. wrote the first complete draft of the manuscript. All authors gave input at various stages during writing.

Funding

Competing interests

The authors declare no competing interests.

Additional information

Supplementary information The online version contains supplementary material available at https://doi.org/10.1038/s41893-023-01159-9.

Correspondence and requests for materials should be addressed to Thomas M. Schutzius.

Peer review information *Nature Sustainability* thanks Zuankai Wang, Xiaoyi Liu and the other, anonymous, reviewer(s) for their contribution to the peer review of this work.

Reprints and permissions information is available at www.nature.com/reprints.

Publisher's note Springer Nature remains neutral with regard to jurisdictional claims in published maps and institutional affiliations.

nature portfolio

Corresponding author(s): Thomas Schutzius

Last updated by author(s): Apr 21, 2023

Reporting Summary

Nature Portfolio wishes to improve the reproducibility of the work that we publish. This form provides structure for consistency and transparency in reporting. For further information on Nature Portfolio policies, see our Editorial Policies and the Editorial Policy Checklist.

Statistics

For all statistical analyses, confirm that the following items are present in the figure legend, table legend, main text, or Methods section.

n/a	Confirmed	
☐	☒	The exact sample size (*n*) for each experimental group/condition, given as a discrete number and unit of measurement
☐	☒	A statement on whether measurements were taken from distinct samples or whether the same sample was measured repeatedly
☐	☒	The statistical test(s) used AND whether they are one- or two-sided *Only common tests should be described solely by name; describe more complex techniques in the Methods section.*
☐	☒	A description of all covariates tested
☐	☒	A description of any assumptions or corrections, such as tests of normality and adjustment for multiple comparisons
☐	☒	A full description of the statistical parameters including central tendency (e.g. means) or other basic estimates (e.g. regression coefficient) AND variation (e.g. standard deviation) or associated estimates of uncertainty (e.g. confidence intervals)
☒	☐	For null hypothesis testing, the test statistic (e.g. *F*, *t*, *r*) with confidence intervals, effect sizes, degrees of freedom and *P* value noted *Give P values as exact values whenever suitable.*
☒	☐	For Bayesian analysis, information on the choice of priors and Markov chain Monte Carlo settings
☐	☒	For hierarchical and complex designs, identification of the appropriate level for tests and full reporting of outcomes
☒	☐	Estimates of effect sizes (e.g. Cohen's *d*, Pearson's *r*), indicating how they were calculated

Our web collection on statistics for biologists contains articles on many of the points above.

Software and code

Policy information about availability of computer code

Data collection	ImageJ bundled with 64-bit Java 8 was used to plot the histograms to find the mean Intensity of the Epiflourescent and color images used for the analysis in the paper.
Data analysis	Microsoft excel was used to analyse the data

For manuscripts utilizing custom algorithms or software that are central to the research but not yet described in published literature, software must be made available to editors and reviewers. We strongly encourage code deposition in a community repository (e.g. GitHub). See the Nature Portfolio guidelines for submitting code & software for further information.

Data

Policy information about availability of data

All manuscripts must include a data availability statement. This statement should provide the following information, where applicable:

- Accession codes, unique identifiers, or web links for publicly available datasets
- A description of any restrictions on data availability
- For clinical datasets or third party data, please ensure that the statement adheres to our policy

All data required to to interpret, verify and extend the research in the article are provided and mentioned through a link in the manuscript.

Human research participants

Policy information about [studies involving human research participants and Sex and Gender in Research.](#)

Reporting on sex and gender
> *Use the terms sex (biological attribute) and gender (shaped by social and cultural circumstances) carefully in order to avoid confusing both terms. Indicate if findings apply to only one sex or gender; describe whether sex and gender were considered in study design whether sex and/or gender was determined based on self-reporting or assigned and methods used. Provide in the source data disaggregated sex and gender data where this information has been collected, and consent has been obtained for sharing of individual-level data; provide overall numbers in this Reporting Summary. Please state if this information has not been collected. Report sex- and gender-based analyses where performed, justify reasons for lack of sex- and gender-based analysis.*

Population characteristics
> *Describe the covariate-relevant population characteristics of the human research participants (e.g. age, genotypic information, past and current diagnosis and treatment categories). If you filled out the behavioural & social sciences study design questions and have nothing to add here, write "See above."*

Recruitment
> *Describe how participants were recruited. Outline any potential self-selection bias or other biases that may be present and how these are likely to impact results.*

Ethics oversight
> *Identify the organization(s) that approved the study protocol.*

Note that full information on the approval of the study protocol must also be provided in the manuscript.

Field-specific reporting

Please select the one below that is the best fit for your research. If you are not sure, read the appropriate sections before making your selection.

☐ Life sciences   ☐ Behavioural & social sciences   ☐ Ecological, evolutionary & environmental sciences

For a reference copy of the document with all sections, see [nature.com/documents/nr-reporting-summary-flat.pdf](#)

Life sciences study design

All studies must disclose on these points even when the disclosure is negative.

Sample size
> *Describe how sample size was determined, detailing any statistical methods used to predetermine sample size OR if no sample-size calculation was performed, describe how sample sizes were chosen and provide a rationale for why these sample sizes are sufficient.*

Data exclusions
> *Describe any data exclusions. If no data were excluded from the analyses, state so OR if data were excluded, describe the exclusions and the rationale behind them, indicating whether exclusion criteria were pre-established.*

Replication
> *Describe the measures taken to verify the reproducibility of the experimental findings. If all attempts at replication were successful, confirm this OR if there are any findings that were not replicated or cannot be reproduced, note this and describe why.*

Randomization
> *Describe how samples/organisms/participants were allocated into experimental groups. If allocation was not random, describe how covariates were controlled OR if this is not relevant to your study, explain why.*

Blinding
> *Describe whether the investigators were blinded to group allocation during data collection and/or analysis. If blinding was not possible, describe why OR explain why blinding was not relevant to your study.*

Behavioural & social sciences study design

All studies must disclose on these points even when the disclosure is negative.

Study description
> *Briefly describe the study type including whether data are quantitative, qualitative, or mixed-methods (e.g. qualitative cross-sectional, quantitative experimental, mixed-methods case study).*

Research sample
> *State the research sample (e.g. Harvard university undergraduates, villagers in rural India) and provide relevant demographic information (e.g. age, sex) and indicate whether the sample is representative. Provide a rationale for the study sample chosen. For studies involving existing datasets, please describe the dataset and source.*

Sampling strategy
> *Describe the sampling procedure (e.g. random, snowball, stratified, convenience). Describe the statistical methods that were used to predetermine sample size OR if no sample-size calculation was performed, describe how sample sizes were chosen and provide a rationale for why these sample sizes are sufficient. For qualitative data, please indicate whether data saturation was considered, and what criteria were used to decide that no further sampling was needed.*

Data collection	*Provide details about the data collection procedure, including the instruments or devices used to record the data (e.g. pen and paper, computer, eye tracker, video or audio equipment) whether anyone was present besides the participant(s) and the researcher, and whether the researcher was blind to experimental condition and/or the study hypothesis during data collection.*
Timing	*Indicate the start and stop dates of data collection. If there is a gap between collection periods, state the dates for each sample cohort.*
Data exclusions	*If no data were excluded from the analyses, state so OR if data were excluded, provide the exact number of exclusions and the rationale behind them, indicating whether exclusion criteria were pre-established.*
Non-participation	*State how many participants dropped out/declined participation and the reason(s) given OR provide response rate OR state that no participants dropped out/declined participation.*
Randomization	*If participants were not allocated into experimental groups, state so OR describe how participants were allocated to groups, and if allocation was not random, describe how covariates were controlled.*

Ecological, evolutionary & environmental sciences study design

All studies must disclose on these points even when the disclosure is negative.

Study description	*Briefly describe the study. For quantitative data include treatment factors and interactions, design structure (e.g. factorial, nested, hierarchical), nature and number of experimental units and replicates.*
Research sample	*Describe the research sample (e.g. a group of tagged Passer domesticus, all Stenocereus thurberi within Organ Pipe Cactus National Monument), and provide a rationale for the sample choice. When relevant, describe the organism taxa, source, sex, age range and any manipulations. State what population the sample is meant to represent when applicable. For studies involving existing datasets, describe the data and its source.*
Sampling strategy	*Note the sampling procedure. Describe the statistical methods that were used to predetermine sample size OR if no sample-size calculation was performed, describe how sample sizes were chosen and provide a rationale for why these sample sizes are sufficient.*
Data collection	*Describe the data collection procedure, including who recorded the data and how.*
Timing and spatial scale	*Indicate the start and stop dates of data collection, noting the frequency and periodicity of sampling and providing a rationale for these choices. If there is a gap between collection periods, state the dates for each sample cohort. Specify the spatial scale from which the data are taken*
Data exclusions	*If no data were excluded from the analyses, state so OR if data were excluded, describe the exclusions and the rationale behind them, indicating whether exclusion criteria were pre-established.*
Reproducibility	*Describe the measures taken to verify the reproducibility of experimental findings. For each experiment, note whether any attempts to repeat the experiment failed OR state that all attempts to repeat the experiment were successful.*
Randomization	*Describe how samples/organisms/participants were allocated into groups. If allocation was not random, describe how covariates were controlled. If this is not relevant to your study, explain why.*
Blinding	*Describe the extent of blinding used during data acquisition and analysis. If blinding was not possible, describe why OR explain why blinding was not relevant to your study.*

Did the study involve field work? ☒ Yes ☐ No

Field work, collection and transport

Field conditions	The experiments were done from July 2022 and January 2023 between 10:00 and 16:00 (UTC+02:00). The outdoor temperature ranged from 25 °C to 33 °C and 8 °C to 9 °C, respectively. Besides the UV index of the solar radiation varied on average between 5-7 in July and 0-1 in January (a value of 10 + being extreme).
Location	The outdoor fog setup on the roof of a building at ETH Zurich, Switzerland (latitude 47.377747, longitude 8.547607)
Access & import/export	The roof was accessible
Disturbance	There were no disturbance

Reporting for specific materials, systems and methods

We require information from authors about some types of materials, experimental systems and methods used in many studies. Here, indicate whether each material, system or method listed is relevant to your study. If you are not sure if a list item applies to your research, read the appropriate section before selecting a response.

Materials & experimental systems		Methods	
n/a	**Involved in the study**	**n/a**	**Involved in the study**
☒ ☐	Antibodies	☒ ☐	ChIP-seq
☒ ☐	Eukaryotic cell lines	☒ ☐	Flow cytometry
☒ ☐	Palaeontology and archaeology	☒ ☐	MRI-based neuroimaging
☒ ☐	Animals and other organisms		
☒ ☐	Clinical data		
☒ ☐	Dual use research of concern		